



ARTICLE

Effects of Filler-Asphalt Ratio on the Properties of Lignin and Polyester Fiber Reinforced SMPU/SBS Modified Asphalt Mortar

Wenjing Xia^{1,*}, Jinhui Wang¹, Tao Xu¹ and Nan Jiang²

¹College of Civil Engineering, Nanjing Forestry University, Nanjing, 210037, China

²College of Civil Engineering, Yancheng Institute of Technology, Yancheng, 224051, China

*Corresponding Author: Wenjing Xia. Email: wjxia@njfu.edu.cn

Received: 07 October 2022 Accepted: 05 December 2022 Published: 26 June 2023

ABSTRACT

To understand the effects of filler-asphalt ratio on different properties of lignin and polyester fiber reinforced shape memory polyurethane (SMPU)/styrene butadiene styrene (SBS) composite modified asphalt mortar (PSAM), as well as to reveal the reinforcing and toughening mechanisms of lignin and polyester fibers on PSAM, SMPU, SBS and mineral powder were first utilized to prepare PSAM. Then the conventional, rheological and anti-cracking properties of lignin fiber reinforced PSAM (LFAM) and polyester fiber reinforced PSAM (PFAM) at different filler-asphalt ratios were characterized. Test results indicate that the shear strength, deformation resistance and viscosity are increased after adding 0.8wt% lignin fiber or polyester fiber and increasing the filler-asphalt ratio from 0.8 to 1.2. The optimal filler-asphalt ratio of 1.0 is proposed after comprehensive performance assessments of PSAM. Polyester fiber shows a better reinforcing effect than lignin fiber, but its improvement in the thermal stability of PSAM is not significant at high temperatures. Additionally, the complex modulus, storage modulus, loss modulus and rutting resistance factor of PSAM are improved after adding lignin fiber and polyester fiber, as well as show an increasing trend as the filler-asphalt ratio is raised, but the phase angle is gradually decreased. Further, the increase of elastic components in PSAM effectively enhances the anti-deformation ability of PSAM at high temperatures, and polyester fiber more obviously improves the high-temperature deformation resistance of PSAM than lignin fiber. Finally, the anti-cracking performance of PFAM and LFAM at low temperatures is reduced by 74.2% and 46.7%, respectively, as the filler-asphalt ratio is raised from 0.8 to 1.2. The low-temperature anti-cracking performance of LFAM is lower than that of PFAM at the same filler-asphalt ratio, even lower than that of PSA. Compared with lignin fiber, the anti-cracking performance and deformation resistance of PSAM at low temperature is more greatly enhanced by polyester fiber.

KEYWORDS

Asphalt mortar; fiber reinforcement; filler-asphalt ratio; anti-cracking performance; high-temperature stability; deformation resistance

1 Introduction

Recently, the demand for pavement construction is constantly increasing as road transportation is rapidly developing. Asphalt pavement is widely used on highways and urban roads because of its better skid resistance, smoother surface, lower noise, comfortable driving, easier maintenance, and convenient



recycling [1]. There into, there is a significant impact of asphalt mortar on the pavement properties of asphalt pavement such as high-temperature rutting resistance, anti-cracking performance at low temperatures and water stability. Asphalt mortar is a kind of micro-dispersion system, in which the filler is the dispersed phase and distributed in the continuous phase of asphalt [2]. Asphalt mortar theory points out that asphalt mixture is the spatial network structure, and asphalt mortar has an obvious impact on the pavement performance of the asphalt mixture [3]. However, according to previous studies [4], the properties of asphalt mortar affected the deformation resistance, anti-cracking performance, anti-aging ability, fatigue resistance and water stability of asphalt mixture. Therefore, it is necessary to investigate the properties of asphalt mortar to improve the service performance and durability of asphalt pavement.

As is known to all, the modulus of mineral filler particles is larger than those of asphalt, and the particle size of the filler is small, while the specific surface area of the filler is large. The mineral filler particle has strong physical adsorption with asphalt, and even the chemical reaction between filler and asphalt also occurs. With the increase in filler content, the dispersion or aggregation state of filler affects asphalt mortar properties, and then affects asphalt mixture properties [5], so the researches on various properties of asphalt mortar have attracted much attention.

Nie et al. found that the design of asphalt mortar could coordinate the anti-cracking and rutting resistance of the asphalt mixture to improve its comprehensive pavement performance [5]. In addition, they proposed the critical values of technical indicators of asphalt mortar, which not only guaranteed the high-temperature stability to meet the technical requirements of asphalt mixture, but also raised its good deformation resistance ability. Zhao et al. investigated the effects of different fine aggregate sizes on the creep properties of asphalt mortar using numerical and test methods, as well as found that fine aggregate sizes in the range of 0.15–0.3 mm were important ones [6]. Ran et al. used oil sludge pyrolysis residue to substitute mineral powder to prepare asphalt mortar, as well as pointed out that silane coupling agent facilitated strong chemical and physical adsorptions between asphalt and filler, so which improved different properties of asphalt mortar [7]. Davoodi et al. utilized rubber powder and nano-silica to prepare asphalt mortar for reducing the creep stiffness of asphalt mortar, as well as reported rubber mortar and nano-silica showed great effects on the mechanical and service properties of semi-flexible pavement [8].

To further improve the anti-cracking performance at low temperatures, high-temperature stability and water stability of asphalt mortar, various fibers are frequently mixed into asphalt mortar to enhance the mechanical properties of asphalt mortar. The commonly used fibers are lignin fiber, mineral fiber and polymer fiber. The existing researches show that the added fibers in asphalt can effectively exert the reinforcement and adsorption effects on asphalt, as well as inhibit the expansion of microcrack and prolong the service life of asphalt mortar [9]. Some studies found that fiber played a certain role in reinforcing asphalt due to its surface properties and adsorption, improving the anti-rutting ability and anti-shear performance of asphalt pavement at high temperatures. Nevertheless, there was a decreasing effect on the viscosity after reaching a certain content of fiber [10].

Some studies also validated that the ductility of modified asphalt was reduced as the fiber content was raised, which lowered the cracking resistance at low temperatures of the asphalt mixture, and asphalt pavement crack was not reduced at low temperatures [11]. Gu et al. evaluated the effects of five filler-binder ratios, four fiber types, five fiber contents and three fiber lengths on the rheological performance of asphalt mortar [12]. They reported that basalt fiber greatly enhanced the rheological properties of asphalt mortar at high temperatures, and strengthened stress dissipation. Slebi-Acevedo et al. investigated the reinforcing effects of polyacrylonitrile fiber and polyolefin-aramid fiber on asphalt mortar using indirect tensile tests, and found the fibers had significant improvement in mechanical strength [13]. Qian et al. examined the reinforcing effects of various fibers on asphalt mortar and reported that the added polyester fiber significantly enhanced the mechanical properties of asphalt mortar [14]. Marvila et al. studied the

application of natural fibers in cementitious composites and pointed out the alkaline pretreatment of fiber improved its adhesion properties, durability, water absorption and tensile strength [15]. Azevedo et al. used the natural pineapple fiber in the eco-friendly mortar to repair crack, and found the natural fiber with 2.5wt% content improved the technological properties and durability of mortar [16].

At present, the mechanical and rheological properties of modified asphalt mortar were investigated. However, the effects of filler-asphalt ratio on different properties of lignin and polyester fiber reinforced shape memory polyurethane (SMPU)/styrene butadiene styrene (SBS) composite modified asphalt mortar (PSAM) were seldom discussed. Further, a single type of fiber was often used to reinforce asphalt mortar, but the reinforcing and toughening effects of granular lignin fiber and linear polyester fiber on PSAM were rarely compared. The reinforcing and toughening mechanisms of the above two fibers on the mechanical, rheological and service properties of PSAM were not fully revealed. Therefore, the objective of this work is to understand the effects of filler-asphalt ratio on different properties of lignin and polyester fiber reinforced PSAM, and reveal the reinforcing and toughening mechanisms of lignin and polyester fibers on PSAM. This may effectively increase the shape recovery force, self-healing ability and pavement performance of PSAM, prolonging the service life of asphalt pavement.

In this work, the two typical lignin fiber and polyester fiber with large specific surface areas and better adsorption properties were selected as the reinforcing and toughening materials of PSAM. Firstly, PSAM samples with different filler-asphalt ratios were prepared. The softening point test, cone penetration test and viscosity test were used to study the effects of different filler-asphalt ratios and fiber types on the conventional properties of PSAM. Then the bending beam rheometer (BBR) test and dynamic shear rheometer (DSR) test were conducted to further analyze the effects of filler-asphalt ratios and fiber types on the rheological and anti-cracking properties of PSAM. Thus, the impacts of fiber type and filler content on various properties of PSAM were evaluated, revealing the reinforcing and toughening mechanisms of lignin fiber and polyester fiber on PSAM.

2 Materials and Methods

2.1 Materials

The raw materials were polyadipic acid-1,4-butanediol ester (PBAG), 1,4-butanediol (BDO), 4,4-diphenylmethane diisocyanate (MDI), glycerol (GLY), SBS modifier and matrix asphalt with a 60/80 penetration grade. PBAG was bought from Asahikawa Chemical Co., Ltd., Suzhou, China. MDI was provided by Xiya Chemistry Industry Ltd., Shandong, China. BDO and GLY were produced from Sinopharm Chemical Reagent Co., Ltd., China. SBS was provided by Diansheng Industry Co., Ltd., Jiangxi, China. Matrix asphalt was supplied by Lucky Gold Chemicals Co., Ltd., Tianjin, China. The penetration of matrix asphalt was 65.2 dmm, the ductility at 5°C was 15.5 cm and the softening point was 54.7°C. The limestone powder was provided by Building Materials Co., Ltd., Anhui, China. Its fundamental properties were tested according to Chinese Test Methods of Aggregate for Highway Engineering (JTG E42-2005) and Technical Specifications for Construction of Highway Asphalt Pavements (JTG F40-2004). The fundamental properties of limestone powder were listed in Table 1.

Table 1: Fundamental properties of limestone powder

Test items	Technical standard	Test results	Test methods
Particle size range	<0.6 mm(%)	100	T0351
	<0.015 mm(%)	90–100	
	<0.075 mm(%)	75–100	
Apparent density (g/cm ³)	≥2.5	2.681	T0352

(Continued)

Table 1 (continued)			
Test items	Technical standard	Test results	Test methods
Hydrophilic coefficient	<1	0.7	T0353
Plasticity index	<4	1.9	T0354
Appearance	Agglomerate without aggregates	Agglomerate without aggregates /	

The polyester fiber was polytrimethylene terephthalate (PTT) fiber, and was purchased from Tianyi Engineering Fiber Co., Ltd., Jiangsu, China. The length of PTT fiber was 6 mm, its diameter was 23 μm , its density was 1.33 g/cm^3 , its tensile strength is 517 MPa, and its oil absorption rate was 6.5%.

The lignin fiber was provided by Chenqi Chemical Technology Co., Ltd., Shanghai, China. The length of lignin fiber was 300 μm , its bulk density was 260 g/L , its drying loss rate was less than 5%, its pH value was 7, and its water absorption rate was 8.5%.

2.2 Preparation of Fiber Reinforced PSAM

2.2.1 Preparation of PSA Sample

The preparation method of SMPU/SBS composite modified asphalt (PSA) was as follows:

Firstly, the calculated amount of partial PBAG was put into the four-mouth flask equipped with a vacuum connected catheter stirrer and thermometer. The flask was heated to 120°C on an electric heating jacket. Then the remaining PBAG was added and dehydrated under the vacuum conditions at -0.1 MPa for 2 h. After that, the temperature was cooled to 80°C, and the MDI was mixed to react for 2 h after stirring at 800 rpm. Thus, the SMPU prepolymer with the mass ratio of PBAG/BDO/MDI = 1:4:3 was prepared.

Secondly, matrix asphalt was heated to the flow state at 160°C, and was sheared for 10 min at 1500 rpm using a shearing machine. The SBS modifier which accounted for 3% of asphalt mass was added slowly, and was fully swollen by continuing to shear for 15 min. Then the blend was sheared at 180°C and 5000 rpm for 30 min and developed for 2 h at 180°C to prepare SBS modified asphalt.

Thirdly, SBS modified asphalt was heated to the flow state in an oven at 160°C. Then it was cooled to 120°C and stabilized. A certain amount of prepared SMPU prepolymer was added into SBS modified asphalt, and was stirred at 1000 rpm for 60 min. Next, BDO was mixed based on the ratio of PBAG, BDO and MDI for chain extension for 5 min. The calculated amount of GLY was added to cross-link for 5 min.

Finally, the stirring speed of the above mixture was adjusted to 3000 rpm. The blend was sheared for 20 min, and then placed in an oven at 120°C for 2 h to prepare PSA.

2.2.2 Preparation of LFAM or PFAM Sample

The preparation method of the LFAM or PFAM sample was as follows:

(1) The limestone powder was heated in the oven for 4 h at 105°C, and about 300 g PSA was heated to the flow state in the oven at 160°C.

(2) In the light of JTG F40-2004, the commonly used filler-asphalt ratio range was 0.8–1.2. In this paper, the asphalt mortar samples were prepared with the three filler-asphalt ratios of 0.8, 1.0 and 1.2. The required limestone mineral powder filler was weighed.

(3) The prepared asphalt was added into the beaker. When the heating jacket temperature was raised to about 160°C, the mineral filler was added slowly into the beaker. The glass rod was used to manually stir the mixture to prevent uneven heating of asphalt and uneven distribution of mineral filler until no mineral filler floated on the asphalt surface. At the same time, the high-speed shear machine was preheated to around 160°C.

(4) The lignin fiber or polyester fiber was added which accounts for 0.8% of asphalt mass, respectively, as well as were manually stirred until all fibers were evenly dispersed in asphalt and no air bubbles were produced.

(5) The shear machine was utilized to mix and stir for 20 min at 2000 rpm to obtain the lignin fiber reinforced PSAM (LFAM) sample or polyester fiber reinforced PSAM (PFAM) sample, respectively.

2.3 Methods

2.3.1 Cone Penetration Test

The penetration test method of asphalt was not feasible to test the consistency of asphalt mortar. Hence, the fine needle in the penetration tester was replaced with a machined cone needle as shown in Fig. 1.

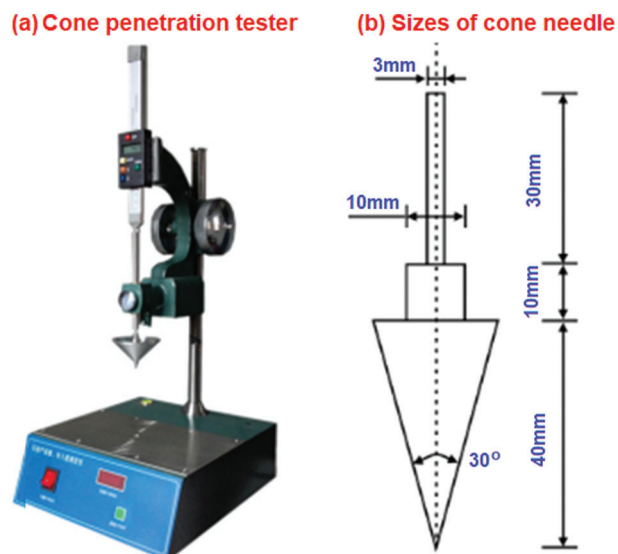


Figure 1: Cone penetration tester and the sizes of cone needle

The penetration tester was converted to the cone penetration tester, and the temperature of cone penetration test was 25°C which was the same as the penetration test method. The penetration duration was 5 s. The shear strength could be calculated by Eq. (1) based on the cone penetration test results 5.

$$\tau = \frac{981Q\cos^2(\partial/2)}{\pi h^2 \tan(\partial/2)} \quad (1)$$

where Q was the penetration mass (185 g), τ was the shear strength (KPa), h was the cone penetration (0.1 mm), and ∂ was the cone needle tip angle (30°).

2.3.2 Softening Point Test

To make sure the phase change temperature, temperature sensitivity and high-temperature stability of asphalt mortar, the softening point of asphalt mortar was measured based on the Chinese Standard Test

Methods of Asphalt and Asphalt Mixtures for Highway Engineering (JTG E20-2011). A high softening point indicated that asphalt mortar had better thermal stability at high temperatures.

2.3.3 Brookfield Viscosity Test

The Brookfield viscosity test of asphalt mortar was conducted on a Brookfield viscosity analyzer at 135°C based on JTG E20-2011. Because asphalt mortar was a highly viscous fluid, the rotation speed was set at 20 rpm to investigate the viscosity changes of asphalt mortar with different filler-asphalt ratios.

2.3.4 DSR Test

The rheological property of asphalt mortar at high temperatures was characterized by the DSR test. The test frequency (ω) was 10 rad/s. The strain value (γ) was 12%. The test temperature was 64°C. The specimen thickness and diameter were 1 mm and 25 mm, respectively. The rutting factor ($G^*/\sin\delta$) of asphalt mortar was measured to study the rheological properties of asphalt mortar at high temperatures.

2.3.5 BBR Test

The low-temperature bending property of asphalt mortar was investigated by the BBR test. The prepared specimen sizes of asphalt mortar were 127 mm in length, 6.35 mm in thickness and 12.7 mm in width. The 0.980 N load was applied on the beam for 240 s. The displacement sensor was utilized to test the deflection. The creep stiffness (S) and creep slope (m) in double logarithmic coordinates at 60 s were chosen as the evaluation indexes.

2.3.6 AFM Test

AFM (Multimode 8, Bruker, Germany) was utilized to characterize the microscopic morphology of crack surfaces of LFAM and PFAM specimens. The imaging mode adopted the tapping method to intuitively study the fiber distribution and reinforcement effect in PSAM. The microscopic morphology changes of crack surfaces in LFAM and PFAM specimens were characterized at the nano-microscopic scale. The scanning rate was set to 1 Hz, and the pre-pressure was 30 nN, and the scanning size was $20 \mu\text{m} \times 20 \mu\text{m}$ for each sample.

3 Results and Discussions

3.1 Basic Performance Analysis of PASM

3.1.1 Effects of Filler-Asphalt Ratio on the Shear Strength of LFAM and PFAM

To investigate the changes in cone penetration and shear strength of LFAM and PFAM at different filler-asphalt ratios, the cone penetration tests are carried out on LFAM and PFAM. The results are provided in Fig. 2.

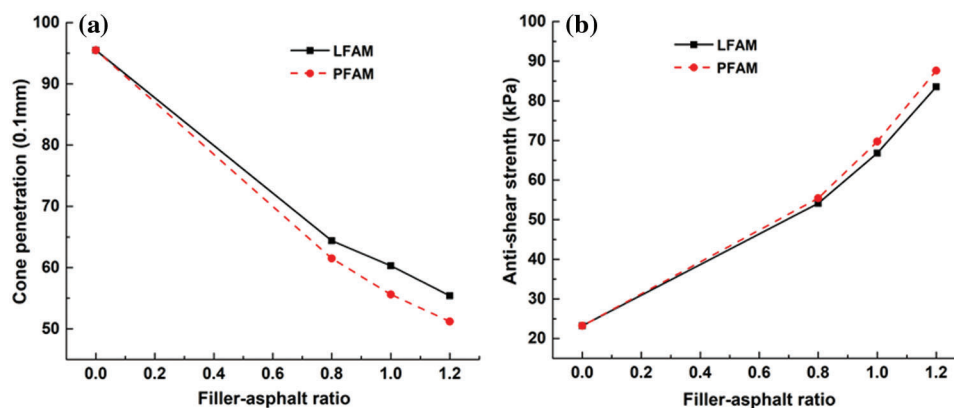


Figure 2: (a) Test results of cone penetration and (b) shear strength of LFAM and PFAM at different filler-asphalt ratios

From Fig. 2a, the cone penetration of LFAM decreased significantly from 9.55 mm to 6.44 mm, 6.03 mm and 5.54 mm, as well as the cone penetration of PFAM decreased from 9.55 mm to 6.15 mm, 5.56 mm and 5.12 mm at the filler-asphalt ratios of 0.8, 1.0 and 1.2, respectively. However, the shear strength of PSA is 23.2 kPa. The highest shear strengths of LFAM and PFAM are 83.5 kPa and 87.6 kPa at the filler-asphalt ratio of 1.2, respectively, showing a significant increase in shear strength. This indicates that the added fibers serve as the reinforcing and bridging roles in PSAM [17]. The reason is that the physical and chemical interactions occur between fibers and asphalt, such as adsorption, diffusion, chemical bonding, etc. Hence, asphalt is arranged on the surface of fibers in the monomolecular form, forming the interfacial layer of structural asphalt with a strong bonding force. Also, the interfacial effect between the PSAM phase and mineral filler phase is increased, leading to an increase in the shear strength of LFAM and PFAM, which improves the shear resistance of PFAM.

From Fig. 2b, comparing the test results of LFAM and PFAM at the same fiber content and filler-asphalt ratio, the PFAM has a lower cone penetration and larger shear strength, leading to a greater shear deformation resistance. Further, at the filler-asphalt ratio of 1.2, the PFAM has a lower cone penetration of 5.12 mm than the LFAM of 5.54 mm, but the shear strength of PFAM is 87.6 KPa, which is higher than that of LFAM. The shear strength is a reflection of the reinforcing effect of fibers on PSAM, and the reinforcing effect is more related to the morphology of the fibers themselves [18]. The shear resistance of PSAM is enhanced by fibers with appropriate length and shape. The lignin fibers are vegetable fibers with a cotton-like appearance and various lengths. The linear long polyester fibers are macromolecular polymer fibers, which are similar in length and shape. The inherent mechanical properties of polyurethane fibers are higher than those of lignin fibers, so the shear strength of PFAM is better than that of LFAM.

From Fig. 2, the cone penetration of the same fiber reinforced PSAM at each filler-asphalt ratio is decreased, but the anti-shear strength is raised with the increase in filler content. Whether it is LFAM or PFAM, the cone penetration is decreased by about 1 cm and the anti-shear strength is increased by about 20 kPa as the filler-asphalt ratio is changed from 0.8 to 1.2. This indicates that as the mineral filler content is increased, PSAM becomes thicker and harder, as well as the adsorption to asphalt is increased, eventually forming a dense and uniformly dispersed spatial network structure with better integrity and improved shear resistance. The shear resistance is increased as the filler-asphalt ratio becomes higher. Therefore, the high-temperature stability of PSAM can be increased by appropriately raising the filler-asphalt ratio.

3.1.2 Impacts of Filler-Asphalt Ratio on the High-Temperature Stability of LFAM and PFAM

To investigate the temperature sensitivity and high-temperature stability of LFAM and PFAM at different filler-asphalt ratios, the softening point tests are carried out on both LFAM and PFAM, and the results are given in Fig. 3.

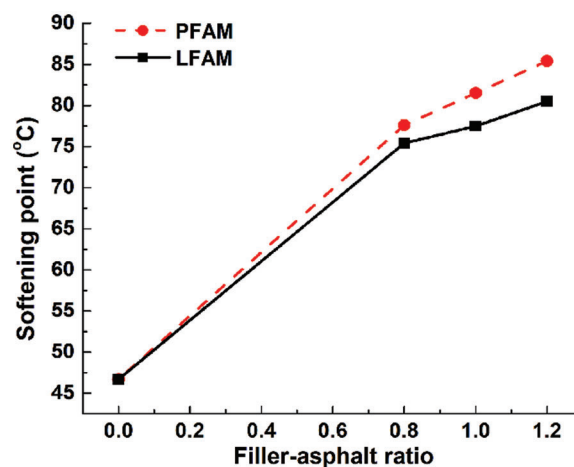


Figure 3: Softening point test results of LFAM and PFAM at different filler-asphalt ratios

From Fig. 3, after adding different types of fibers, the softening point of PSAM is increased from 46.7°C to 75°C, and the increased amplitude of softening point is more than 60%. The larger softening point indicates a higher equiviscous temperature and better high-temperature stability of PSAM. On the one hand, the particle size of limestone mineral powder is smaller, so the mineral powder content is raised when the filler-asphalt ratio is increased. The mineral powder adsorbs more asphalt to form thicker structural asphalt, which thickens and hardens the PSAM, reducing the temperature sensitivity of PSAM and improving its high-temperature stability [19]. On the other hand, the lignin fibers and polyester fibers are distributed in PSAM in a three-dimensional phase. The surface of fibers absorbs the light oil components in PSAM, transforming the unstable sol-gel structure into a more stable gel structure. This results in a better reinforcement effect on PSAM and improves its high-temperature stability of PSAM [20].

By comparing the softening points of LFAM and PFAM when the filler-asphalt ratio is the same, it is found that the softening points of PFAM are higher than those of LFAM at the three filler-asphalt ratios. Further, the softening point of PFAM is 77°C when the filler-asphalt ratio is 0.8, while the softening point of LFAM is 77.6°C at the filler-asphalt ratio of 1.0, which is close to that of PFAM at the filler-asphalt ratio of 0.8, but the mineral powder content is higher than that of LFAM. This is because the evenly dispersed polyester fibers in the PSAM form an obvious three-dimensional network structure with high toughness and possess a strong interfacial bonding force with the asphalt matrix due to the higher oil absorption characteristics [12]. This forms a stable three-dimensional system and enhances the toughness of PFAM, leading to an increase in the high-temperature thermal stability of PFAM.

Additionally, the macromolecular chains in SMPU and SBS are also interpenetrated to form a spatial network in PFAM. The more compact composite network structure is formed by polyester fibers and macromolecular chain interpenetration, further significantly enhancing the thermal stability of PFAM. Nevertheless, the granular lignin fibers are difficult to form three-dimensional network structures in LFAM, increasing the thermal stability at high temperatures. Therefore, the softening points of PFAM are higher than those of LFAM at the three filler-asphalt ratios, but the difference in softening point of PFAM and LFAM is also not significant because the contents of lignin fiber and polyester fiber only account for 0.8% of asphalt mass, respectively.

Finally, from Fig. 3, the softening point tends to increase steadily as the filler-asphalt ratio is raised, but this increasing trend is not obvious. As the filler-asphalt ratio is increased from 0.8 to 1.2, the softening point of LFAM and PFAM is increased in a gradient of about 5%, showing an insignificant increasing trend. Compared with the above analysis results, the softening point is increased by 60% at the filler-asphalt ratio of 0.8, which shows that the thermal stability of asphalt is increased due to the added mineral powder and fibers. However, the improvement effect is not so obvious in the filler-asphalt ratio range of 0.8–1.2 [21].

3.1.3 Influence of Filler-Asphalt Ratio on the Viscosity of LFAM and PFAM

To investigate the viscosity changes of LFAM and PFAM at different filler-asphalt ratios, Brookfield viscosity tests are conducted on LFAM and PFAM at different filler-asphalt ratios as illustrated in Fig. 4.

From Fig. 4, the viscosity values of PFAM are larger than those of LFAM at the three filler-asphalt ratios. Especially, the viscosity value of PSA is 0.5 Pa·s, and the viscosity values of LFAM and PFAM are 13.6 kPa·s and 15.9 kPa·s corresponding to the filler-asphalt ratio of 0.8, respectively. The viscosity values of both LFAM and PFAM are larger than 30 kPa·s at the filler-asphalt ratio of 1.2. The viscosity of PSAM is obviously increased after adding the fibers and more mineral powder. The primary reasons are that the limestone powder has higher physical adsorption to asphalt components, causing the increase in the viscosity of PSAM as the limestone powder content is raised.

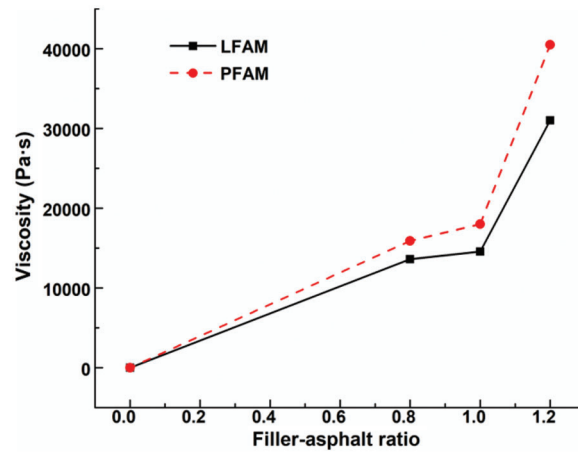


Figure 4: Brookfield viscosity test results of LFAM and PFAM at different filler-asphalt ratios

Secondly, comparing the viscosity values of LFAM and PFAM at the same filler-asphalt ratio, the viscosity value of PFAM is larger than that of LFAM at the three different filler-asphalt ratios. Especially, at the filler-asphalt ratio of 1.2, the viscosity value of PFAM reaches 40.5 kPa·s at 135°C, which is higher than that of LFAM by 30%. The reasons are that the polyester fibers are randomly distributed in PSAM to act as the overlap joints and reinforcements, forming a three-dimensional network with PSAM and mineral powder. These structures produce a larger internal frictional resistance under the action of external load. Besides, polyester fibers are products derived from petroleum, and it has strong similarity with petroleum asphalt. According to the similar compatibility principle, the polymer fiber has a strong interfacial effect and high adsorption to asphalt, so its promotion effect of adhesion on PSAM viscosity is obvious [22].

Also, the length and toughness of macromolecular polyester fiber are larger than those of lignin fiber [23]. These make macromolecular polyester fiber have better adhesive properties with PSAM. Hence, the viscosity improvement of polyester fiber on PSAM is more noticeable. All these factors make PFAM become a more dense and compact micro-dispersion system, which is reflected macroscopically by an increase in viscosity. This agrees with the test results of cone penetration and softening point. It is concluded that polyester fiber has a higher viscosity enhancement effect on PSAM than lignin fiber.

Finally, from Fig. 4, the viscosity values of LFAM and PFAM are increased as the mineral powder content is raised, but the increased amplitude is different. As the filler-asphalt ratio is increased from 0.8 to 1.0, the viscosity value is increased by 6.9%–13.2%. However, as the filler-asphalt ratio is raised from 1.0 to 1.2, the viscosity value is increased significantly by 113.1%–125.0%. It is seen that the viscosity of PSAM is not only related to fiber type, but also is greatly relevant to the filler-asphalt ratio. The effect of filler on the viscosity index of PSAM becomes more evident as the filler content is raised. However, the workability of the asphalt mixture is decreased by the excessive viscosity in the actual asphalt pavement construction, so it is important to choose a suitable filler-asphalt ratio range of 0.8–1.2.

3.2 Rheological Properties of LFAM and PFAM at Different Filler-Asphalt Ratios

To discuss the rheological properties of LFAM and PFAM at different filler-asphalt ratios at high temperatures, DSR tests are carried out on LFAM and PFAM as provided in Figs. 5 and 6.

As illustrated in Fig. 5, the G^* of PSAM is increased and the δ is reduced because of the addition of the two types of fibers and mineral powder. Firstly, the G^* of PSA is 3.9 kPa, but the G^* of LFAM and PFAM are significantly increased after the addition of fibers and mineral powder. As the filler-asphalt ratio is raised, the

G^* values of LFAM and PFAM are also increased, and the highest G^* values of LFAM and PFAM are 32.1 kPa and 65.5 kPa as the filler-asphalt ratio of 1.2, respectively. This is because there is a surface-active acid in PSAM, which forms an integral structural layer by physical absorption and chemical bonding with the added fibers. During the DSR test, the tentacled fibers disperse the load on the PSAM, resulting in an increase in the G^* and bearing capacity [24].

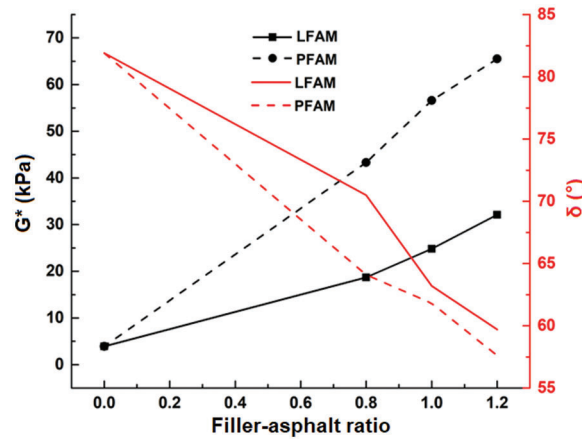


Figure 5: Test results of complex modulus and phase angle of LFAM and PFAM at different filler-asphalt ratios

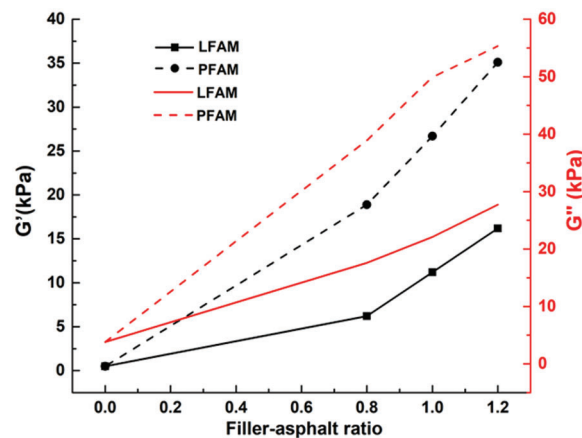


Figure 6: Test results of storage modulus and loss modulus of LFAM and PFAM at different filler-asphalt ratios

Next, the limestone mineral powder is evenly dispersed in the PSA to adsorb asphalt and to fill the voids, so that the G^* tends to increase due to the double-action of both fibers and mineral powder. Then, compared with the δ of PSA, the δ values of both LFAM and PFAM show a decreasing trend. The δ of LFAM is decreased from 70.5° to 59.7° and the δ of PFAM is decreased from 64.1° to 57.6° , which are both lower than that of PSA (81.9°). It indicates that the δ of PSAM is reduced by the addition of fibers, and the elastic component of PSAM is increased, resulting in the stronger mechanical properties of PSAM [25].

The changes in the loss modulus (G'') and storage modulus (G') of LFAM and PFAM at different filler-asphalt ratios are given in Fig. 6.

From Fig. 6, both G' and G'' of PSAM are increased after the addition of fibers and mineral powder. The G' and G'' of PSA are 0.5 kPa and 3.8 kPa, but the G' and G'' of PSAM are significantly increased after the addition of fibers. Further, the G' of PFAM is 35.1 kPa and the G'' is 55.7 kPa when the filler-asphalt ratio is 1.2. This is because the elastic components in PSAM are increased by the addition of fibers, and the G' reflects the energy storage and energy release in the deformation process of PSAM. The increase in elastic component leads to an increase in G' [26].

The G'' reflects the dissipated energy in the form of thermal energy generated by internal friction during the deformation of PSAM, which is the unrecoverable part of PSAM after the deformation. However, the viscosity is improved because of the absorption and bonding of mineral powder and fiber with PSA components. Also, it is found that the unrecoverable part and the loss modulus become larger as the filler-asphalt ratio is increased. These are consistent with the representation of loss modulus, and it also agrees with the above analysis results of viscosity tests.

Additionally, from Fig. 6, the rising trend of G'' is linear, while the rising trend of G' is almost exponential, and the rising trend of G'' is weaker than that of G' . It is because phase separation occurs during the deformation, and the response ability of viscosity is always weaker than that of the elasticity due to the large cohesion. Therefore, during the mechanical changes in viscoelastic materials, the thermodynamic response of viscous phase separation always lags behind that of elastic components [27].

From Fig. 7, $G^*/\sin\delta$ is significantly increased after adding fibers and mineral powder. $G^*/\sin\delta$ is also increased as the filler-asphalt ratio is raised. In fact, PSA acts together with the mineral powder and fibers to resist the external force during the deformation. The lowest values of $G^*/\sin\delta$ for LFAM and PFAM are 19.8 kPa and 48.1 kPa, respectively, which are 5 times and 12 times larger than the $G^*/\sin\delta$ of PSAM. This indicates that the deformation resistance of PSAM at high temperatures is enhanced by the added fibers, which is similar with the test results of cone penetration.

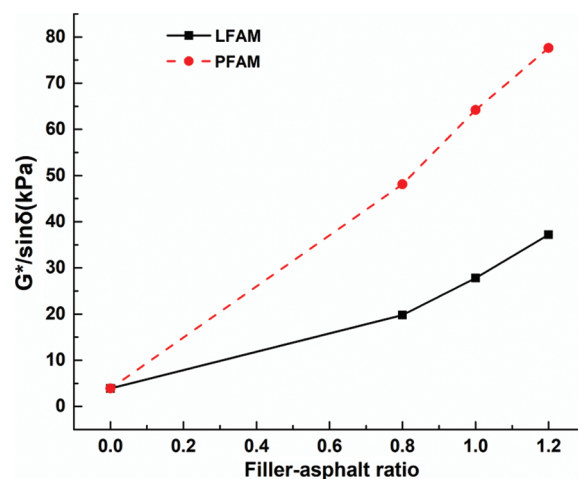


Figure 7: Test results of $G^*/\sin\delta$ of LFAM and PFAM at different filler-asphalt ratios

From Fig. 7, $G^*/\sin\delta$ is increased as the filler-asphalt ratio is raised, as well as the curve shape of $G^*/\sin\delta$ is not identical for LFAM and PFAM as the filler-asphalt ratio is raised. Under the same test conditions, although the filler-asphalt ratio is increased in the form of an equal gradient, the variation amplitude of $G^*/\sin\delta$ is different. This is related to the dispersion uniformity of multiphase materials after mixing, and is also closely related to the characteristics of the material itself.

Finally, the $G^*/\sin\delta$ of PFAM is higher than that of LFAM at the same filler-asphalt ratio, and is almost twice that of LFAM. It is because the polyester fiber is uniform in shape and size, as well as better aligned and

has higher toughness and oil absorption [28]. These allow polyester fiber to become more compatible with asphalt than lignin fiber, and the combination between polyester fibers and PSA provides better high-temperature deformation resistance for PSAM.

From Fig. 7, after the addition of fibers and mineral powder, the $G^*/\sin\delta$ of PSAM is obviously increased, and the increased amplitude is noticeable. The $G^*/\sin\delta$ of PSAM is significantly increased as the filler-asphalt ratio is raised. At the same filler-asphalt ratio, the $G^*/\sin\delta$ of PFAM is larger than that of LFAM at the same fiber content, suggesting that polyester fiber shows a better reinforcing effect than lignin fiber to increase the deformation resistance at high temperatures.

3.3 Anti-Cracking Performance of LFAM and PFAM at Different Filler-Asphalt Ratios

To investigate the anti-cracking performance of LFAM and PFAM at different filler-asphalt ratios at low temperatures, BBR tests are carried out on LFAM and PFAM as given in Figs. 8–10.

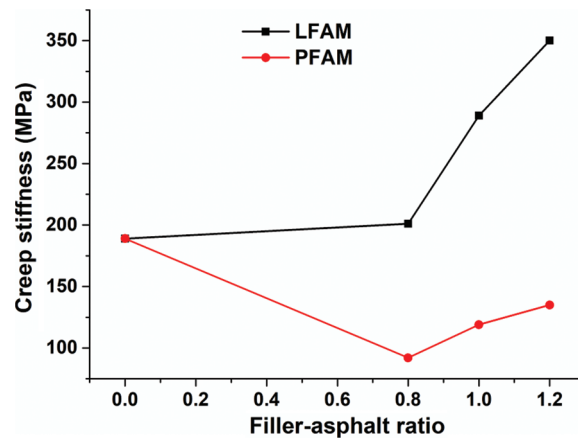


Figure 8: The results of creep stiffness of LFAM and PFAM at different filler-asphalt ratios

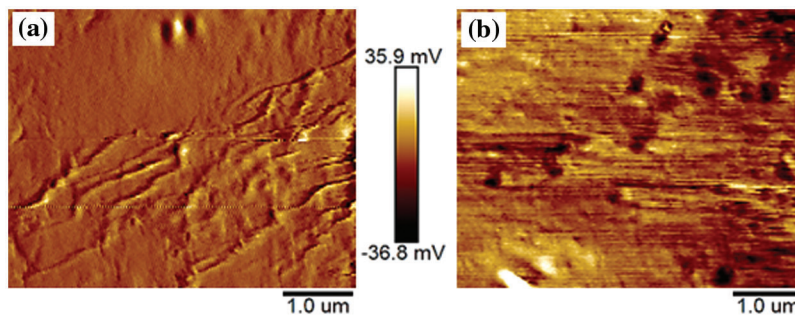


Figure 9: The AFM images of crack surfaces of (a) LFAM and (b) PFAM

As shown in Fig. 8, the creep stiffness of PSA is 189 MPa, which is higher than those of PFAM at the three filler-asphalt ratios, but is lower than those of LFAM. The creep stiffness represents the flexibility of PSAM, and the smaller creep stiffness indicates better anti-cracking performance at low temperatures. This is because the dislocation and movement of mineral powder particles are limited by the added fibers, which reduces the generation of cracks, and hinders the development of cracks, enhancing the flexibility of PSAM. Additionally, the lignin fiber mainly plays the filling role in the LFAM, as well as its reinforcing and toughening effects are not obvious. The LFAM specimen shows a brittle failure at low temperatures, and its crack surface is smoother as shown in Fig. 9a. However, the mechanical properties

of polyester fiber are much better than those of lignin fiber, as well as the adhesive force between polyester fibers and the PSAM matrix causes the PFAM to become more flexible through the pull-out action from the PSAM matrix as shown in Fig. 9b. Hence, the low-temperature crack resistance of PFAM is better than that of LFAM. As illustrated in Fig. 8, the creep stiffness of PFAM is lower than that of LFAM.

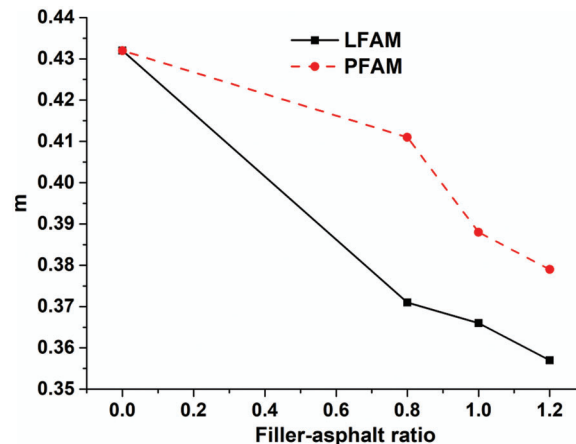


Figure 10: Test results of m values of LFAM and PFAM at different filler-asphalt ratios

From Fig. 8, the creep stiffness values of LFAM and PFAM are the lowest ones at the filler-asphalt ratio of 0.8, suggesting that their low-temperature anti-cracking properties are the best ones. When compared with the creep stiffness of PSA, the creep stiffness of LFAM is still higher than that of PSA. Besides, as the filler-asphalt ratio is increased, insufficient mixing may lead to the uneven dispersion of mineral powder in PSA, so that some uncoated mineral powder particles cannot form continuous structural asphalt. This reduces the bonding properties of PSA, resulting in a brittle failure of PSA mortar at low temperatures and increasing the stiffness modulus. As a result, LFAM has a higher creep stiffness than PSA.

Also, as the filler-asphalt ratio is raised, the creep stiffness of PFAM is decreased, and is lower than that of LFAM as the filler-asphalt ratio is the same one, and even is lower than that of PSA. It suggests that the cracking resistance of PFAM is much better than that of LFAM. The reason is that when compared with lignin fiber, polyester fiber has better low-temperature anti-cracking performance, and belongs to the same kind of polymer as SMPU. According to the similarity compatibility principle, polyester fiber has better interfacial bonding with asphalt and SMPU. Next, the polyester fiber has strong absorption to PSA, so it is mixed evenly with PSAM, which plays an effective role in reinforcing PSAM to disperse and bear partial stress, so as to effectively improve the anti-cracking performance of PSAM at low temperatures. It is concluded that the added mineral powder reduces the anti-cracking performance of PFAM and LFAM at low-temperature, as well as their anti-cracking properties are decreased by 74.2% and 46.7%, respectively, as the filler-asphalt ratio is raised from 0.8 to 1.2.

From Fig. 10, the creep slope (m) is used to characterize the relaxation performance of PSAM. The PSAM has faster stress release rate, stronger relaxation capacity and larger creep slope value, indicating it has better low-temperature anti-cracking performance. The creep slope value of PSA is 0.432, which is not obviously different from the creep slope values of LFAM and PFAM at the three filler-asphalt ratios. This is because the creep stiffness of mineral powder is the smallest one, but its creep slope is the largest one. Also, the increase in fiber content has little effect on the stress accumulation of PSAM, resulting in little change in creep slope value. These reflect that the fiber has little influence on the stress accumulation ability of PSAM, so there is little change in creep slope value.

4 Conclusions

Based on the above test and analysis results, the major conclusions are obtained as follows:

(1) Both polyester fiber and lignin fiber reduce the cone penetration of PSAM. The cone penetration of PFAM is more obviously decreased. Both polyester fiber and lignin fiber increase the shear strength of PSAM. The shear strength of PFAM is more greatly increased and has a stronger shear resistance. The shear strength of PSAM is increased as the filler-asphalt ratio is raised, and the anti-deformation ability of PSAM is improved by appropriately increasing the filler-asphalt ratio.

(2) The high-temperature stability of PSAM is improved by adding polyester fiber and lignin fiber. There is little difference between polyester fiber and lignin fiber in increasing the softening point of PSAM. Also, when the filler-asphalt ratio is raised, the increased amplitude of softening point is small, indicating that the filler-asphalt ratio shows no significant effect on the improvement of high-temperature stability of LFAM and PFAM.

(3) The viscosity of PSAM is improved by increasing the filler-asphalt ratio, as well as by adding lignin fiber and polyester fiber. The polyester fiber shows a more obvious enhancement effect on the viscosity of PSAM than lignin fiber. At the filler-asphalt ratio range of 0.8–1.0, the viscosity of PSAM is little changed with the increase in filler content, but at the filler-asphalt ratio of 1.0–1.2, the viscosity of PSAM is greatly changed. The appropriate filler-asphalt ratio range is 0.8–1.2. After comprehensive performance assessments, the optimal filler-asphalt ratio of 1.0 is proposed.

(4) The complex modulus, storage modulus, loss modulus and rutting resistance factor of PSAM are increased significantly by adding lignin fiber, polyester fiber and mineral powder, as well as show an increasing trend as the filler-asphalt ratio is raised, but the phase angle is gradually decreased. The elastic component in PSAM is increased, improving the mechanical properties and deformation resistance of PSAM. Moreover, polyester fiber better improves the deformation resistance of PSAM than lignin fiber.

(5) The added mineral powder reduces the anti-cracking performance of PFAM and LFAM at low-temperature, as well as their anti-cracking properties are decreased by 74.2% and 46.7%, respectively, as the filler-asphalt ratio is raised from 0.8 to 1.2. The low-temperature deformation resistance of LFAM is lower than that of PFAM at the same filler-asphalt ratio, and even is lower than that of PSA. Compared with lignin fiber, polyester fiber more significantly improves the cracking resistance and anti-deformation of PSAM at low temperatures.

Funding Statement: This work was supported by National Natural Science Foundation of China (No. 52208440), Natural Science Foundation of Jiangsu Province (BK20210618), the Natural Science Foundation of the Jiangsu Higher Education Institutions of China (21KJB580003) and National Undergraduate Training Program for Innovation and Entrepreneurship (2021NFUSPITP0638).

Conflicts of Interest: The authors declare that they have no conflicts of interest to report regarding the present study.

References

1. Ren, S. S., Liu, X. Y., Xu, J., Lin, P. (2021). Investigating the role of swelling-degradation degree of crumb rubber on CR/SBS modified porous asphalt binder and mixture. *Construction and Building Materials*, 300(11), 124048. <https://doi.org/10.1016/j.conbuildmat.2021.124048>
2. Xu, L., Shang, P., Xu, X. W., Herrick, A. M., Sgro, A. et al. (2011). Studies on synthesis and properties of novel polyurethane pavement joint sealant modified with polydimethylsiloxane. *Material Research Innovations*, 15(2), 150–155. <https://doi.org/10.1179/143307511X12998222919119>

3. Zhu, S., Fu, Q., Cai, C., Spanos, P. D. (2022). Damage evolution and dynamic response of cement asphalt mortar layer of slab track under vehicle dynamic load. *Science China Technological Sciences*, 57(10), 1883–1894. <https://doi.org/10.1007/s11431-014-5636-8>
4. Hidei, V., Sidun, L., Hunyak, O., Stanchak, S., Bidos, V. (2020). Application of wastepaper sludge ash as mineral powder for hot asphalt concrete mix. *Theory and Building Practice*, 2(2), 42–47. <https://doi.org/10.23939/jtbp2020.02.042>
5. Nie, G. H., Cai, X., Huang, W. K., Hassan, H. M., Chen, S. et al. (2022). Designing of an anti-rutting and high ductility asphalt mixture based on mortar performance. *Construction and Building Materials*, 316(3), 125837. <https://doi.org/10.1016/j.conbuildmat.2021.125837>
6. Zhao, S., You, Q., Sesay, T. (2022). Fine aggregate sizes effects on the creep behavior of asphalt mortar. *Construction and Building Materials*, 342(2), 127931. <https://doi.org/10.1016/j.conbuildmat.2022.127931>
7. Ran, W., Zhu, H., Shen, X., Zhang, Y. (2022). Rheological properties of asphalt mortar with silane coupling agent modified oil sludge pyrolysis residue. *Construction and Building Materials*, 329(11), 127057. <https://doi.org/10.1016/j.conbuildmat.2022.127057>
8. Davoodi, A., Esfahani, M. A., Bayat, M., Mohammadyan-Yasouj, S. E., Rahman, A. (2022). Influence of nano-silica modified rubber mortar and EVA modified porous asphalt on the performance improvement of modified semi-flexible pavement. *Construction and Building Materials*, 337(2), 127573. <https://doi.org/10.1016/j.conbuildmat.2022.127573>
9. Wu, B., Pei, Z., Luo, C., Xia, J., Chen, C. et al. (2022). Effect of different basalt fibers on the rheological behavior of asphalt mortar. *Construction and Building Materials*, 318(2), 125718. <https://doi.org/10.1016/j.conbuildmat.2021.125718>
10. Ren, D., Liu, Y., Muhammad, Y., Li, X. Y., Mao, C. et al. (2022). Preparation of double-layer film modified polyacrylonitrile fiber modifier for designing and performance evaluation of PAN/SBS composite asphalt. *Construction and Building Materials*, 350(10), 128920. <https://doi.org/10.1016/j.conbuildmat.2022.128920>
11. Ye, Q., Wu, S., Chen, Z., Liu, Z. F. (2008). Rheological properties of asphalt mixtures containing various fibers. *Journal of Central South University of Technology*, 15(S1), 333–336. <https://doi.org/10.1007/s11771-008-0375-2>
12. Gu, Q., Kang, A., Li, B., Xiao, P., Ding, H. (2022). Effect of fiber characteristic parameters on the high and low temperature rheological properties of basalt fiber modified asphalt mortar. *Case Studies in Construction Materials*, 17(1), e01247. <https://doi.org/10.1016/j.cscm.2022.e01247>
13. Slebi-Acevedo, C. J., Lastra-González, P., Castro-Fresno, D., Bueno, M. (2020). An experimental laboratory study of fiber-reinforced asphalt mortars with polyolefin-aramid and polyacrylonitrile fibers. *Construction and Building Materials*, 248, 118622. <https://doi.org/10.1016/j.conbuildmat.2020.118622>
14. Qian, S., Ma, H., Feng, J., Yang, R., Huang, X. (2014). Fiber reinforcing effect on asphalt binder under low temperature. *Construction and Building Materials*, 61(1), 120–124. <https://doi.org/10.1016/j.conbuildmat.2014.02.035>
15. Marvila, M. T., Rocha, H. A., Azevedo A.R., G., Colorado, H. A., Zapata, J. F. et al. (2021). Use of natural vegetable fibers in cementitious composites: Concepts and applications. *Innovative Infrastructure Solutions*, 6(3), 180. <https://doi.org/10.1007/s41062-021-00551-8>
16. Azevedo, A. R. G., Marvila, M. T., Antunes, M. L. P., Rangel, E. C., Fediuk, R. (2021). Technological perspective for use the natural pineapple fiber in mortar to repair structures. *Waste and Biomass Valorization*, 12(9), 5131–5145. <https://doi.org/10.1007/s12649-021-01374-5>
17. Yao, L., Lu, Y., Zhang, C., Yang, S., Yang, C. (2022). Sizing carbon fiber by in situ polymerization of maleic acid and glycerol for reinforcing polyamide 66. *Journal of Applied Polymer Science*, 139(24), 52328. <https://doi.org/10.1002/app.52328>
18. Wang, P., Zhang, H., Cao, Y., Pan, A. Q., Wu, W. (2022). Additively manufactured short carbon fiber reinforced polyetheretherketone by coating polyetherimide at the interface using fused filament fabrication. *Journal of Applied Polymer Science*, 139(26), e52438. <https://doi.org/10.1002/app.52438>
19. Muniandy, R., Aburkaba, E., Taha, R. (2013). Effect of mineral filler type and particle size on the engineering properties of stone mortar asphalt pavements. *Australian Journal of Basic & Applied Sciences*, 7(133), 475–487.

20. Yan, J., Zhou, H., Li, S. (2019). Study on fatigue self-healing properties of basalt fiber asphalt mixture. *Journal of Physics: Conference Series*, 1168(2), 22048.
21. Kou, C., Wu, X., Xiao, P., Liu, Y., Zhu, Z. (2020). Physical, rheological, and morphological properties of asphalt reinforced by basalt fiber and lignin fiber. *Materials*, 13(11), 2520. <https://doi.org/10.3390/ma13112520>
22. Gruber, S., Plank, J. (2020). Preparation and effectiveness of a high-temperature anti-settling agent for well cement slurries. *Journal of Natural Gas Science and Engineering*, 81(2), 103416. <https://doi.org/10.1016/j.jngse.2020.103416>
23. Santos, R., Rossi, P. F., Ramos, L. A., Frollini, E. (2018). Renewable resources and a recycled polymer as raw materials: Mats from electrospinning of lignocellulosic biomass and PET solutions. *Polymers*, 10(5), 538. <https://doi.org/10.3390/polym10050538>
24. Xiang, Y., Xie, Y., Long, G. (2018). Effect of basalt fiber surface silane coupling agent coating on fiber-reinforced asphalt: From macro-mechanical performance to micro-interfacial mechanism. *Construction and Building Materials*, 179, 107–116. <https://doi.org/10.1016/j.conbuildmat.2018.05.192>
25. Xing, X., Chen, S., Li, Y., Pei, J. (2020). Effect of different fibers on the properties of asphalt mastics. *Construction and Building Materials*, 262(8), 120005. <https://doi.org/10.1016/j.conbuildmat.2020.120005>
26. Radaoui, M., Fredj, A. B., Romdhane, S., Bouguerra, N., Egbe, D. A. M. et al. (2022). New conjugated polymer/fullerene nanocomposite for energy storage and organic solar cell devices: Studies of the impedance spectroscopy and dielectric properties. *Synthetic Metals*, 283, 116987. <https://doi.org/10.1016/j.synthmet.2021.116987>
27. Troyani, N. L., Gomes, C. J., Baiz, P. M. (2009). Capability for capturing temperability as a criterion for the validity of thermoviscoelastic constitutive equations. *Journal of Thermal Stresses*, 33(1), 37–54. <https://doi.org/10.1080/01495730903409193>
28. Wong, K. J., Nirmal, U., Lim, B. K. (2010). Impact behavior of short and continuous fiber-reinforced polyester composites. *Journal of Reinforced Plastics and Composites*, 29(23), 3463–3474. <https://doi.org/10.1177/0731684410375639>